


## Article

# Highly Hydrophilic Ti–Beta Zeolite with Ti–Rich Exterior as Efficient Catalyst for Cyclohexene Epoxidation

Huang Pan <sup>1</sup>, Rusi Peng <sup>1</sup>, Zhiguo Zhu <sup>2</sup>, Hao Xu <sup>1,3,\*</sup>, Mingyuan He <sup>1,3</sup> and Peng Wu <sup>1,3,\*</sup> 

<sup>1</sup> Shanghai Key Laboratory of Green Chemistry and Chemical Processes, School of Chemistry and Molecular Engineering, East China Normal University, North Zhongshan Road 3663, Shanghai 200062, China; panhuang1212@163.com (H.P.); rosyuth@163.com (R.P.); myhe@chem.ecnu.edu.cn (M.H.)

<sup>2</sup> Green Chemistry Centre, Department College of Chemistry and Chemical Engineering, Yantai University, 30 Qingquan Road, Yantai 264005, China; zhuzg@ytu.edu.cn

<sup>3</sup> Institute of Eco-Chongming, Shanghai 202162, China

\* Correspondence: hxu@chem.ecnu.edu.cn (H.X.); pwu@chem.ecnu.edu.cn (P.W.)

**Abstract:** Nanocrystalline Ti–Beta zeolite with high hydrophilicity and a Ti–rich exterior was successfully prepared via a dissolution–recrystallization method. With the post–treatment of tetraethylammonium hydroxide (TEAOH) solution at elevated temperature, the Si and Ti species within the Ti–Beta matrix were partially dissolved and recrystallized on the outer surface of crystals, resulting in the Ti–rich exterior and higher hydrophilicity, which improved the accessibility of the active Ti sites and the enrichment of H<sub>2</sub>O<sub>2</sub>. Simultaneously, some of the closed Ti(OSi)<sub>4</sub> species were transformed to more active open Ti(OSi)<sub>3</sub>OH or Ti(OSi)<sub>2</sub>(H<sub>2</sub>O)<sub>2</sub>(OH)<sub>2</sub> species. The modified Ti–Beta zeolite exhibited greatly enhanced catalytic performance in the epoxidation of cyclohexene in comparison to the parent Ti–Beta.

**Keywords:** Ti–Beta; Ti–rich exterior; hydrophilicity; cyclohexene epoxidation



**Citation:** Pan, H.; Peng, R.; Zhu, Z.; Xu, H.; He, M.; Wu, P. Highly Hydrophilic Ti–Beta Zeolite with Ti–Rich Exterior as Efficient Catalyst for Cyclohexene Epoxidation. *Catalysts* **2022**, *12*, 434. <https://doi.org/10.3390/catal12040434>

Academic Editors: Anabela A. Valente and Tiehong Chen

Received: 12 March 2022

Accepted: 10 April 2022

Published: 12 April 2022

**Publisher's Note:** MDPI stays neutral with regard to jurisdictional claims in published maps and institutional affiliations.



**Copyright:** © 2022 by the authors. Licensee MDPI, Basel, Switzerland. This article is an open access article distributed under the terms and conditions of the Creative Commons Attribution (CC BY) license (<https://creativecommons.org/licenses/by/4.0/>).

## 1. Introduction

Epoxy cyclohexane (CHO) serves as an important raw material for the production of a series of high value–added organic compounds [1,2], such as pharmaceutical intermediates, pesticides, resins, surfactants, photosensitive coatings and adhesives [3]. To date, the main industrial synthetic methods of CHO include being separated from light oil, electrochemical synthesis and cyclohexene (CHE) epoxidation [4–6]. The former two methods have some drawbacks such as low purity, poor reactivity, high energy consumption and serious environmental pollution, whereas the cyclohexene epoxidation with hydrogen peroxide (H<sub>2</sub>O<sub>2</sub>) as an oxidant and titanosilicates as a heterogeneous catalyst has relatively low cost and meets the requirements of green and sustainable development. It has become the most promising synthetic method for CHO [7].

The first–generation titanosilicate TS–1 reported by Taramasso et al. in 1983 is the most studied and widely used catalyst in the catalytic oxidation reaction [8]. However, limited by the relatively narrow 10–member ring (10–MR) pores (0.51–0.56 nm) of MFI topology, it is difficult for bulky cyclohexene to access the Ti active sites located within the micropores of TS–1. Therefore, the catalytic performance for the epoxidation of cyclohexene is poor because of the pore blocking and fast deactivation. Afterward, a series of microporous titanosilicates with different framework topologies and larger pore sizes, such as Ti–MWW [9], Ti–MOR [10] and Ti–\*BEA (Ti–Beta) [11], and Ti–containing mesoporous silicas, such as Ti–SBA–15 [12] and Ti–MCM–41 [13], have been reported. Notably, compared with TS–1 and Ti–MWW, Ti–Beta with an external or three–dimensional 12–MR pore system exhibited superior activity in processing relative bulky substrates, such as the epoxidation of cyclohexene [14,15]. However, the synthesis of conventional Ti–Beta zeolite usually contains Al ions, and the Brønsted acid sites generated by the framework

Al ions reduce the activity of Ti–Beta in the epoxidation of olefins. Thus, the synthesis of Al–free systems has been intensively studied. To date, several synthetic methods have been reported for Al–free Ti–Beta zeolites, including hydrothermal synthesis [16–18], dry–gel conversion [11] and post–treatment synthesis [19–21]. Moreover, due to the differences in particle size and hydrophilicity/hydrophobicity of Ti–Beta prepared via different synthetic strategies, the catalytic activity is also distinct. For instance, the Ti–Beta zeolite hydrothermally synthesized with the assistance of F<sup>−</sup> ions possessed micro-sized crystals (>1 μm), which induced severe diffusion constraints and thus poor activity in the cyclohexene epoxidation reaction [17,18,22]. The hydrothermally synthesized Ti–Beta zeolites generally contain a large number of silanol groups due to the intergrowth of polymorphs A and B, which hinders the adsorption of organic molecules, giving rise to poor activity in the epoxidation of cyclohexene [22].

It is generally recognized that the main factors affecting the catalytic activity of Ti–zeolites/H<sub>2</sub>O<sub>2</sub> system are Ti active sites, diffusion limitation and hydrophilicity/hydrophobicity of the zeolite frameworks. In order to further improve the catalytic performance of oxidation reactions involving bulky molecules such as cyclohexene, constructing hierarchical Ti–Beta crystals with intracrystalline mesopores or improving the accessibility of active Ti sites by adjusting the location of titanium species is also an effective strategy [23–25]. At present, the methods for fabricating hierarchical Ti–Beta zeolites mainly include the templating and non–templating methods [26]. Both hard and soft templates can be used in direct synthesis [27,28], while the non–templating methods include post–synthesis [19,29] and recrystallization [30]. You et al. reported a hierarchical Ti–Beta zeolite synthesized with three–dimensional ordered mesoporous carbon as a hard template, and it showed an improved catalytic performance in the cyclohexene epoxidation reaction compared with the conventional Ti–Beta containing sole micropores [27]. Hierarchical Ti–Beta zeolites constructed by Ren et al. using cetyltrimethylammonium bromide as a soft template also showed dramatically improved activity in the epoxidation of cyclohexene and *n*–dodecene [28]. Yu et al. prepared a hierarchical Ti–Beta zeolite with abundant interconnected intracrystalline meso/macropores via a controllable fluoride etching approach. The resultant hierarchical Ti–Beta exhibited remarkably enhanced activity in the oxidative desulfurization of bulky molecules of dibenzothiophene and 4,6–dimethylbenzothiophene, compared to other titanosilicates [31]. Although fabricating hierarchical structures can release the diffusion constraints, the Ti active centers are still mainly located inside zeolite crystals and the substrates need to diffuse inside the pore channels. Thus, concentrating the Ti active centers on the external surface of zeolites would be a more effective method to release the diffusion constraints and improve the utilization efficiency of Ti sites. Additionally, the hydrophilicity/hydrophobicity of titanosilicates is also one of the important factors affecting the catalytic performance. Normally, the hydrophobic Ti–zeolites are expected to achieve high activity in the olefin epoxidation reactions, as it can improve the adsorption capacity of organic substrate molecules. However, Bregante et al. proved that the hydrophilic Ti–Beta showed superior catalytic performance in alkene epoxidation compared to the defect–free hydrophobic Ti–Beta [32]. This was explained by the fact that the disruption of hydrogen–bonded H<sub>2</sub>O clusters anchored to (SiOH)<sub>4</sub> near Ti active sites by the epoxidation transition states could produce entropy gains. Wei et al. proposed that the hydrophilic Ti–Beta is more beneficial for the enrichment of H<sub>2</sub>O<sub>2</sub>, thus facilitating the formation of the active intermediate Ti–OOH species by the interaction of tetrahedrally coordinated Ti species with H<sub>2</sub>O<sub>2</sub> [33]. Therefore, the construction of a highly active Ti–Beta catalyst for the cyclohexene epoxidation reaction by tailoring the location of Ti active sites and hydrophilicity/hydrophobicity is still highly desirable.

In our recently published work, nanosized Ti–Beta with high Ti content was synthesized using the structural reconstruction method [22]. In the present study, a TEOH–assisted post–modification process was performed over this nanosized Ti–Beta zeolite with the aim to enhance the catalytic performance in the epoxidation reaction of bulky cyclohexene. The post–modification conditions, including the H<sub>2</sub>O/Si ratio, TEOH/Si ratio and

treatment temperature, were carefully investigated and determined to achieve higher catalytic activity. Furthermore, a possible modification mechanism was proposed by tracking the post-modification process. The physicochemical properties of Re-Ti-Beta were then analyzed and compared to those of parent Ti-Beta zeolite to give the reason for the enhanced catalytic performance. The catalytic conditions as well as the reusability were also studied for Re-Ti-Beta zeolite to construct a highly active titanosilicate/H<sub>2</sub>O<sub>2</sub> catalytic system for the epoxidation reaction of cyclohexene.

## 2. Results and Discussion

### 2.1. Synthesis of Re-Ti-Beta Catalyst by Post-Modification

The synthesis of Re-Ti-Beta was performed by modifying the nanosized Ti-Beta in the aqueous TEAOH solution at elevated temperature. As the TEAOH solution not only provided an alkaline medium but also served as OSDA, the dissolution of the zeolite framework and the recrystallization process could occur simultaneously in the TEAOH treatment. Thus, the treatment condition would significantly affect the balance between the above-mentioned dissolution and recrystallization process and then the textural and catalytic properties of Re-Ti-Beta. The treatment conditions, including the H<sub>2</sub>O/Si ratio, TEAOH/Si ratio and treatment temperature, were firstly investigated in detail, with the catalytic performance in the cyclohexene epoxidation reaction as the evaluation criterion. As shown in Figure 1A, with the increase in H<sub>2</sub>O/Si ratio, the CHE conversion firstly increased and then decreased. The main product was CHO, together with the by-products of 1,2-cyclohexanediol (CHD) derived from hydrolysis of CHO and cyclohex-2-en-1-ol (CHEL) and cyclohex-2-en-1-one (CHEE) formed by the allylic oxidation of CHE. The increase in H<sub>2</sub>O/Si ratio from 24 to 60 enhanced the CHO selectivity from 80.1% to 86.8% (Figure 2A). The H<sub>2</sub>O/Si ratio affected the alkalinity of the solution in the modification system, and the CHE conversion reached the maximum value when the H<sub>2</sub>O/Si ratio was 36. Then, fixing the H<sub>2</sub>O/Si ratio at 36, the influence of the TEAOH/Si ratio on the catalytic performance of Re-Ti-Beta was further investigated (Figure 1B). With a low TEAOH/Si ratio of 0.04, the CHE conversion decreased obviously compared with the parent Ti-Beta catalyst, probably because the amount of TEAOH was not enough for recrystallization. The CHE conversion gradually increased from 14.0% to 27.9% with an increase in the TEAOH/Si ratio from 0.08 to 0.20. Then, the CHE conversion decreased to 24.9% and 22.6% with a further increase in the TEAOH/Si ratio to 0.24 and 0.28, respectively, probably due to the increased alkalinity with excess TEAOH amount that then resulted in severe structural dissolution. The variation of CHO selectivity with the increase in TEAOH/Si also showed a volcano-shaped trend (Figure 2B). The treatment temperature was varied in the range of 373 to 433 K (Figure 1C). The CHE conversion also showed a volcano-shaped trend with a rising treatment temperature, while the CHO selectivity was almost consistent (Figure 2C). The optimized temperature was 413 K. Therefore, the optimal conditions for the modification of Ti-Beta were determined to be the H<sub>2</sub>O/Si ratio of 36, the TEAOH/Si ratio of 0.20 and the treatment temperature of 413 K.

As has been revealed above, the molar ratio of TEAOH/Si was critical for the structural modification of Ti-Beta zeolite. Thus, the physicochemical properties of Re-Ti-Beta zeolites were further investigated with different TEAOH/Si ratios. As shown in Figure 3A, B, with the TEAOH/Si ratio in the range of 0.04–0.24, the crystallinity of Re-Ti-Beta gradually increased. The crystallinity was very low when the TEAOH/Si ratio was 0.04, which was consistent with the low activity in the cyclohexene epoxidation reaction. The reason for the low crystallinity was due to the extent of structural dissolution surpassing that of recrystallization. With the increase in TEAOH/Si ratio, sufficient TEA<sup>+</sup> ions were provided to direct the recrystallization. Furthermore, the coordination state of Ti species in Re-Ti-Beta samples was also investigated by UV-Vis spectra. The absorption bands in the range of 200–230 nm belong to the tetrahedrally coordinated Ti species in the zeolite framework. More specifically, the band at ~210 nm is attributed to the closed Ti(OSi)<sub>4</sub> species, while the one at ~220 nm is ascribed to open Ti(OSi)<sub>3</sub>OH species [34]. The band at

about 280 nm is due to the open hexa-coordinated Ti species of  $[\text{Ti}(\text{OSi})_2(\text{H}_2\text{O})_2(\text{OH})_2]$  in the framework of zeolites [35], while the anatase phase normally shows a band at  $\sim 320$  nm. As shown in Figure 3C, compared to the pristine Ti-Beta with the main band at 210 nm, the main band of Re-Ti-Beta-0.16 and Re-Ti-Beta-0.20 appeared at about 220 nm, accompanied by a weak shoulder band at 280 nm, revealing that Ti species were mainly in the form of open site  $\text{Ti}(\text{OSi})_3\text{OH}$  species and a small amount of open hexa-coordinated species due to the dissolution of framework Si species. Meanwhile, the Re-Ti-Beta-0.04 showed a more obvious shoulder band at 320 nm, compared with Re-Ti-Beta-0.20, suggesting the anatase phase was produced with a lower TEOAH/Si ratio. As has been frequently reported, the open Ti species are more active than the closed ones [34]. Thus, the existence of more open Ti species contributed to the higher activity of Re-Ti-Beta-0.20 compared to pristine Ti-Beta. Additionally, the amount of TEOAH molecules occluded in Re-Ti-Beta increased reasonably with the increase in TEOAH/Si ratio (Figure 3D).

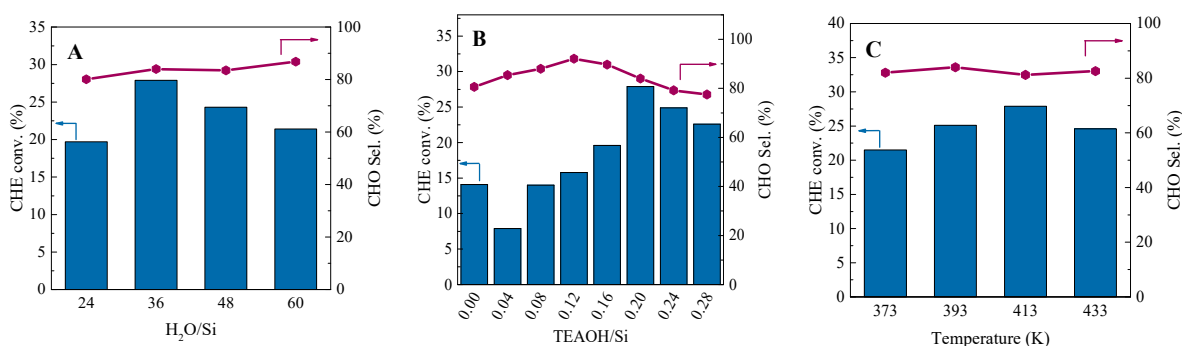


**Figure 1.** Effects of  $\text{H}_2\text{O}/\text{Si}$  molar ratio (A), TEOAH/Si molar ratio (B) and treatment temperature (C) on the catalytic performance of Re-Ti-Beta in cyclohexene epoxidation. Reaction conditions: catalyst, 0.05 g; cyclohexene, 10 mmol;  $\text{H}_2\text{O}_2$  (30 wt.%), 10 mmol; MeCN, 10 mL; temp., 333 K; time, 2 h.

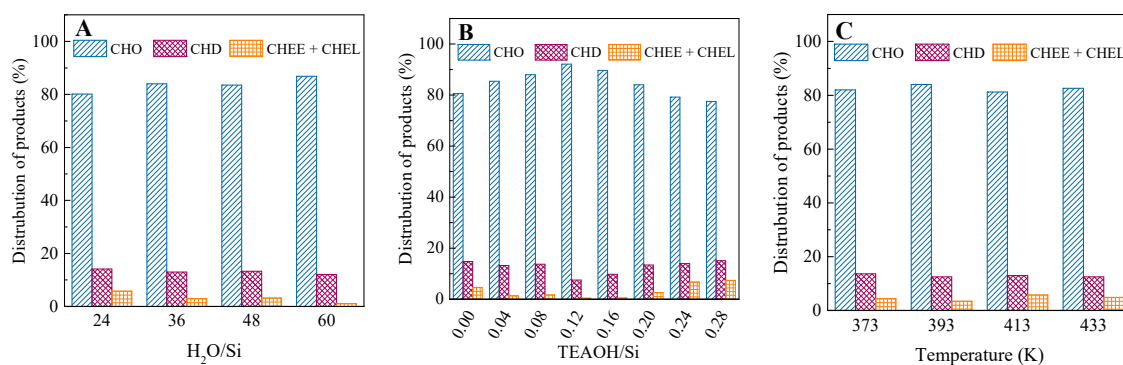


**Figure 2.** Product distribution for cyclohexene epoxidation with Re-Ti-Beta as the catalyst. The Re-Ti-Beta was postsynthesized at different  $\text{H}_2\text{O}/\text{Si}$  molar ratios (A), TEOAH/Si molar ratios (B) and treatment temperatures (C). The products included epoxycyclohexane (CHO), 1,2-cyclohexanediol (CHD), cyclohex-2-en-1-ol (CHEL) and cyclohex-2-en-1-one (CHEE). Reaction conditions: catalyst, 0.05 g; cyclohexene, 10 mmol;  $\text{H}_2\text{O}_2$  (30 wt.%), 10 mmol; MeCN, 10 mL; temp., 333 K; time, 2 h.

To better understand the modification process of Ti-Beta, two typical catalysts of Re-Ti-Beta-0.04 and Re-Ti-Beta-0.20 were further studied. The evolution of structure crystallinity in the TEOAH treatment process, calculated according to the XRD patterns (Figure S1), is shown in Figure 4A. In the modification process of Ti-Beta zeolite via the treatment of TEOAH solution, the  $\text{OH}^-$  groups can dissolve the Beta structure, and the

TEA<sup>+</sup> cations are then able to direct the recrystallization. The relative extent of the structural dissolution and recrystallization affected the structure of Re–Ti–Beta. As shown in Figure S1 and Figure 4A, with the prolonging of treatment time, the crystallinity of the Re–Ti–Beta–0.20 sample increased firstly and then leveled off after 16 h, except for the crystallinity at 8 h. In contrast, the crystallinity of Re–Ti–Beta–0.04 was basically decreased with the increase in crystallization time. The resultant crystallinity of the Re–Ti–Beta–0.20 was slightly higher than that of the pristine Ti–Beta, indicating the extent of recrystallization was larger than that of dissolution. A similar phenomenon has also been reported by Mao et al. in the modification of TS–1 via organic base [36].

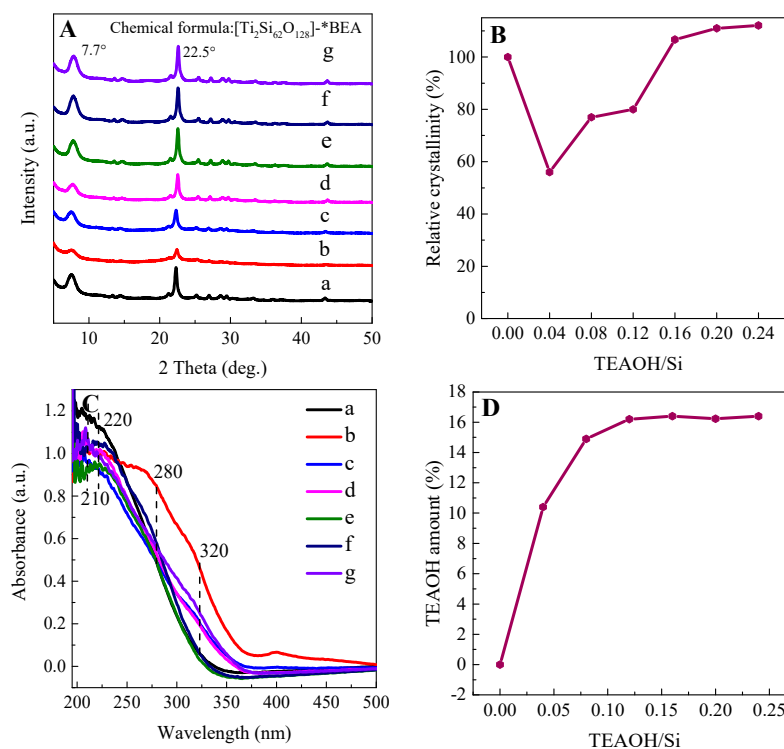


**Figure 3.** XRD patterns (A), crystallinity change (B), UV–Vis spectra (C) and occluded TEAOH amount (D) of the pristine Ti–Beta (a) and Re–Ti–Beta postsynthesized by different TEAOH/Si ratios of 0.04 (b), 0.08 (c), 0.12 (d), 0.16 (e), 0.20 (f) and 0.24 (g).

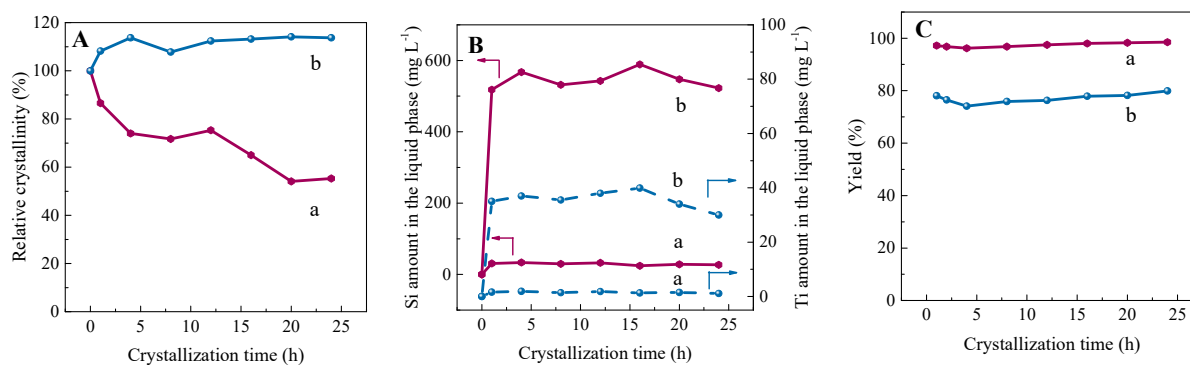


**Figure 4.** The variation of crystallinity (A), the Si (red line) and Ti (blue line) amounts (B) in the liquid phase, and the solid product yield (C) of Re–Ti–Beta–0.04 (a) and Re–Ti–Beta–0.20 (b) with the increase in crystallization time.

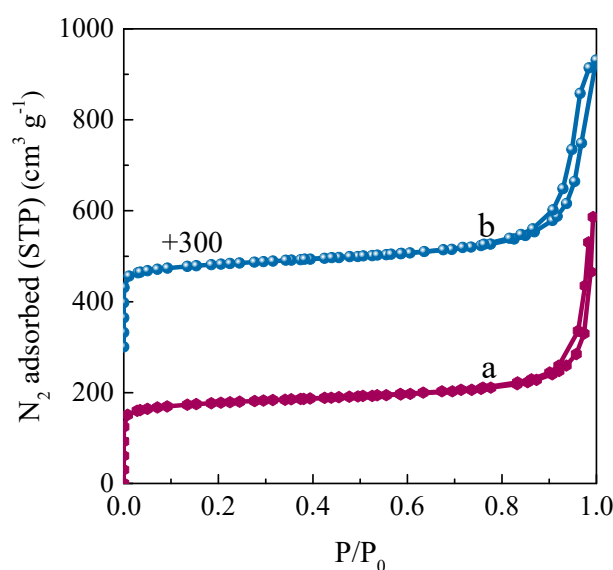
The Si and Ti amounts in the liquid phase of the treatment mixture were investigated during the modification process. As shown in Figure 4B, the Si amount in the

liquid-phase treatment mixture of Re-Ti-Beta-0.20 was ~15-fold higher than that of Re-Ti-Beta-0.04, indicating that more silicon species were dissolved at a higher TEAOH amount. The Ti amount in the liquid-phase treatment mixture of Re-Ti-Beta-0.20 was also higher. The contents of Si and Ti both showed an obvious trend of first increasing and then decreasing for Re-Ti-Beta-0.20, indicating that framework Ti atoms were also dissolved in the alkaline medium and then the dissolved Ti species attended the recrystallization process. However, the yield of Re-Ti-Beta-0.20 (79.9%) was lower than that of Re-Ti-Beta-0.04 (98.5%), as shown in Figure 4C. It is possible that some of the dissolved silicon and titanium species failed to crystallize onto the surface of Re-Ti-Beta-0.20 zeolite and remained in the alkali solution. However, the dissolved Si and Ti species from Re-Ti-Beta-0.04 catalyst might exist in the solid as an amorphous phase, as indicated by the relatively low crystallinity (Figure S1).

## 2.2. Characterization of Catalysts

### 2.2.1. Textural Properties of Re-Ti-Beta Catalyst

Considering the catalytic activity and the crystallinity of the catalysts, Re-Ti-Beta-0.20 was selected for further characterization and compared with the pristine Ti-Beta. The  $N_2$  sorption isotherms of Ti-Beta and Re-Ti-Beta-0.20 are shown in Figure 5. The hysteresis loops appeared at  $0.8 < P/P_0 < 1.0$  in the isotherms of Ti-Beta and Re-Ti-Beta-0.20 due to the presence of intercrystal mesopores. As shown in Table 1, the mesopore volume of Re-Ti-Beta-0.20 increased to  $0.71 \text{ cm}^3 \text{ g}^{-1}$  in comparison to that of Ti-Beta ( $0.62 \text{ cm}^3 \text{ g}^{-1}$ ). The external surface area of Re-Ti-Beta-0.20 was also larger than that of Ti-Beta ( $174 \text{ m}^2 \text{ g}^{-1}$  vs.  $159 \text{ m}^2 \text{ g}^{-1}$ ). The minor enhancement of the pore volume and external surface area helped to release the diffusion constraints of bulky cyclohexene, which also contributed to the increased activity in the epoxidation of cyclohexene. However, it may not be the main reason for the enhanced activity. The SEM images of Ti-Beta and Re-Ti-Beta-0.20 are shown in Figure 6. The pristine Ti-Beta zeolite was composed of nanocrystals with the size of ~50 nm. After the modification with TEAOH solution, the crystal size was decreased, probably because some of the dissolved Si and Ti species failed to crystallize onto the surface of the Ti-Beta crystals. The TEM images of Ti-Beta and Re-Ti-Beta-0.20 further revealed the high crystallinity and the intercrystal mesopores generated by the aggregation of nanosized particles (Figure S2), which was consistent with the results of the  $N_2$  sorption isotherms.

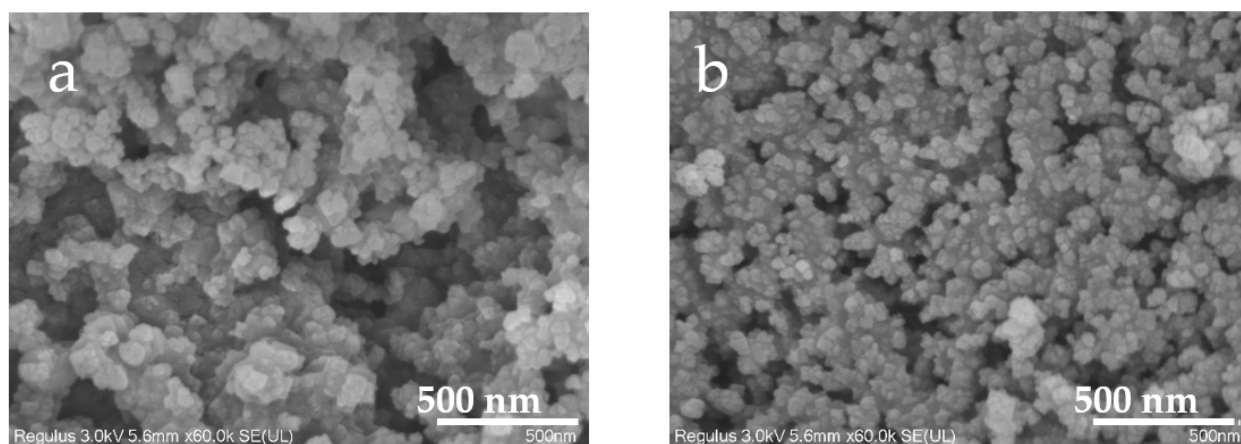


**Figure 5.**  $N_2$  adsorption–desorption isotherms at 77 K of Ti-Beta (a) and Re-Ti-Beta-0.20 (b).

**Table 1.** Textural properties of Ti–Beta and Re–Ti–Beta–0.20.

Sample	Bulk Si/Ti <sup>a</sup>	Surface Si/Ti <sup>b</sup>	SSA (m <sup>2</sup> g <sup>−1</sup> )			Pore volume (cm <sup>3</sup> g <sup>−1</sup> )		
			S <sub>total</sub> <sup>c</sup>	S <sub>micro</sub>	S <sub>ext</sub> <sup>d</sup>	V <sub>total</sub> <sup>c</sup>	V <sub>micro</sub> <sup>d</sup>	V <sub>meso</sub> <sup>e</sup>
Ti–Beta	28.1	102	610	451	159	0.80	0.18	0.62
Re–Ti–Beta–0.20	26.6	57	613	439	174	0.89	0.18	0.71

<sup>a</sup> Determined by ICP. <sup>b</sup> Determined by XPS. <sup>c</sup> Calculated by BET method. <sup>d</sup> Calculated by t–plot method.  
<sup>e</sup> V<sub>meso</sub> = V<sub>total</sub> – V<sub>micro</sub>.

**Figure 6.** The SEM images of Ti–Beta (a) and Re–Ti–Beta–0.20 (b).

### 2.2.2. Coordination State and Location of Ti Active Sites

As shown above in the UV–Vis spectra (Figure 3C), open Ti(OSi)<sub>3</sub>OH and Ti(OSi)<sub>2</sub>(H<sub>2</sub>O)<sub>2</sub>(OH)<sub>2</sub> species were created in the modification process via TEAOH solution. The microenvironment of Ti active sites was further investigated via FT–IR, XPS and UV–Raman spectra. As shown in Figure 7A, the two catalysts exhibited a characteristic band around 960 cm<sup>−1</sup> in FT–IR spectra, which confirmed that the Ti species mainly existed in the Beta framework [37]. In Ti 2p XPS spectra, the peaks at 465.4 and 459.9 eV, corresponding to Ti 2p<sub>1/2</sub> and 2p<sub>3/2</sub>, are attributed to the framework Ti(OSi)<sub>4</sub> species [38]. As shown in Figure 7B, the peak at 459.9 eV was unchanged after modification. However, the peak attributed to Ti 2p<sub>1/2</sub> shifted from 465.6 for Ti–Beta to 465.4 eV for Re–Ti–Beta–0.20. It revealed that the electron cloud density in the outer layer of the framework Ti species slightly increased, which was also related to the formation of Ti(OH)<sub>2</sub>(OSi)<sub>2</sub>(H<sub>2</sub>O)<sub>2</sub> and Ti(OSi)<sub>3</sub>OH species in Re–Ti–Beta–0.20 zeolite [39]. In the UV–Raman spectra of Ti–zeolites, the band at 600–800 cm<sup>−1</sup> is usually assigned to the hexa–coordinated Ti species [40]. The absorption band at 1107 cm<sup>−1</sup> is attributed to the symmetric vibration of Ti–O–Si in zeolite frameworks [41]. As shown in Figure 7C, both Ti–Beta and Re–Ti–Beta–0.20 showed an intense band at 1107 cm<sup>−1</sup> indicative of the framework Ti species. However, a minor band at 720 cm<sup>−1</sup> appeared in the spectrum of Re–Ti–Beta–0.20 zeolite, due to a small amount of open hexa–coordination Ti species, in good agreement with the band at ~280 nm in the UV–Vis spectrum (Figure 3C). Although the coordination state of Ti active sites was altered in the TEAOH treatment, the bulk Si/Ti ratio of Re–Ti–Beta–0.20 was comparable to that of Ti–Beta (Table 1). However, the surface Si/Ti ratio of the Re–Ti–Beta–0.20 was 57, which was lower than that of Ti–Beta, suggesting Ti species were enriched on the external surface of Re–Ti–Beta–0.20. It could be deduced that the dissolved silicon and titanium species in the TEAOH treatment diffused to the crystal surface, and then the recrystallization process occurred under the structural directing effect of TEAOH. In order to verify the Ti–rich exterior of Re–Ti–Beta–0.20, the bulky triphenylamine (TPhA) molecules were used as the poisoning reagent and were considered to selectively poison the active Ti sites on the external surface of Re–Ti–Beta–0.20. The amount of TPhA (2 mmol)

was about 70 times as much as the Ti amount (0.028 mmol) in the two Ti–Beta catalysts, and it should be sufficient to poison the Ti sites that the TPhA molecules could access. As shown in Figure 8, the results showed that the addition of TPhA hardly affected the CHE conversion for Ti–Beta, but the CHE conversion decreased by 34% for Re–Ti–Beta–0.20, suggesting that Re–Ti–Beta–0.20 has more Ti species distributed on the exterior than Ti–Beta. It can be concluded that the enrichment of Ti species on the external surface also contributed to the higher activity of Re–Ti–Beta–0.20 in the epoxidation of bulky cyclohexene by enhancing the accessibility of Ti active sites.

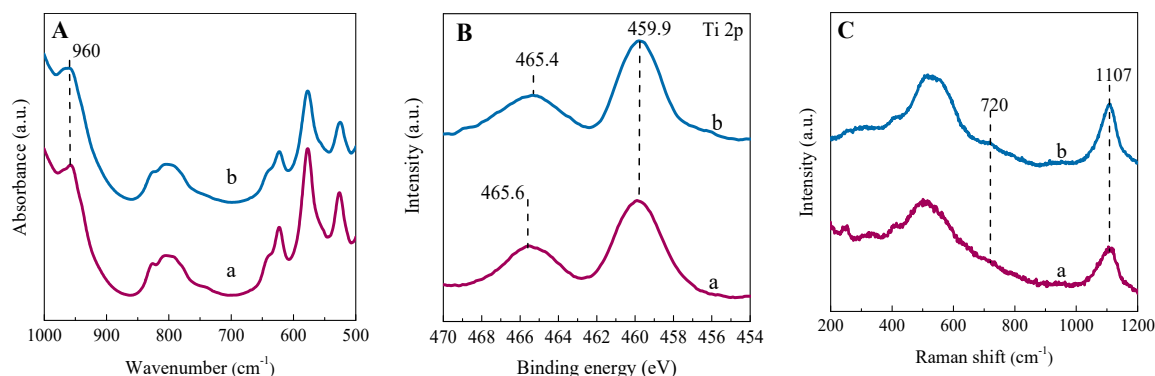


**Figure 7.** FT–IR spectra (A), Ti 2p XPS spectra (B) and UV–Raman spectra (C) of Ti–Beta (a) and Re–Ti–Beta–0.20 (b).

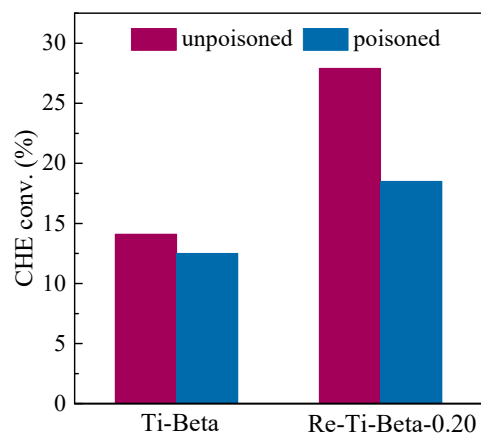


**Figure 8.** The catalytic performance of Ti–Beta and Re–Ti–Beta–0.20 in the cyclohexene epoxidation reaction before and after selective poisoning. Reaction conditions: catalyst, 50 mg; CHE, 10 mmol; H<sub>2</sub>O<sub>2</sub>, 10 mmol; MeCN, 10 mL; TPhA, 2 mmol; temp., 333 K; time, 2 h.

### 2.2.3. Hydrophilicity/Hydrophobicity Property

The appropriate hydrophilicity and hydrophobicity of Ti–zeolites have been proved necessary to achieve high activity and selectivity for the alkene epoxidation reaction with H<sub>2</sub>O<sub>2</sub> [42]. The differences in hydrophilicity/hydrophobicity of the two catalysts were revealed by the H<sub>2</sub>O adsorption isotherms. As shown in Figure 9A, at low values of P/P<sub>0</sub> (<0.2), the isotherms were almost identical for Ti–Beta and Re–Ti–Beta–0.20. However, the uptake of H<sub>2</sub>O on Re–Ti–Beta–0.20 was significantly higher than that of Ti–Beta at higher P/P<sub>0</sub>, which was mainly due to the larger amount of silanols in the former material. The static H<sub>2</sub>O adsorption experiment also showed similar results (Figure S3). The formation of these silanols was supposed to be caused by the structural dissolution in the TEAOH treatment. Therefore, the hydrophilicity of Re–Ti–Beta–0.20 was significantly increased after TEAOH treatment. The FT–IR spectra in the hydroxyl stretching region were also collected to evaluate the amount of silanols semi–quantitatively



(Figure 9B). The band around  $3730\text{ cm}^{-1}$  is attributed to the internal Si–OH, while the band at  $3520\text{ cm}^{-1}$  is ascribed to hydrogen-bonded silanol nests  $(\text{Si}-\text{OH})_4$  [43]. Compared with Ti–Beta, the  $3730$  and  $3520\text{ cm}^{-1}$  bands became more intense for Re–Ti–Beta–0.20 due to the formation of a large number of Ti–OH, Si–OH and  $(\text{Si}-\text{OH})_4$  groups during the modification process. This result was also consistent with the results of  $\text{H}_2\text{O}$  adsorption. Then, the effect of hydrophilicity on  $\text{H}_2\text{O}_2$  adsorption was studied (Figure 9C). The amount of adsorbed  $\text{H}_2\text{O}_2$  over Re–Ti–Beta–0.20 was higher than that of Ti–Beta, indicating that  $\text{H}_2\text{O}_2$  molecules could be effectively enriched in the Re–Ti–Beta–0.20, benefiting from its higher hydrophilicity. Thus, this also contributed to the improved catalytic activity of Re–Ti–Beta–0.20 by enriching  $\text{H}_2\text{O}_2$ , compared to the pristine Ti–Beta.

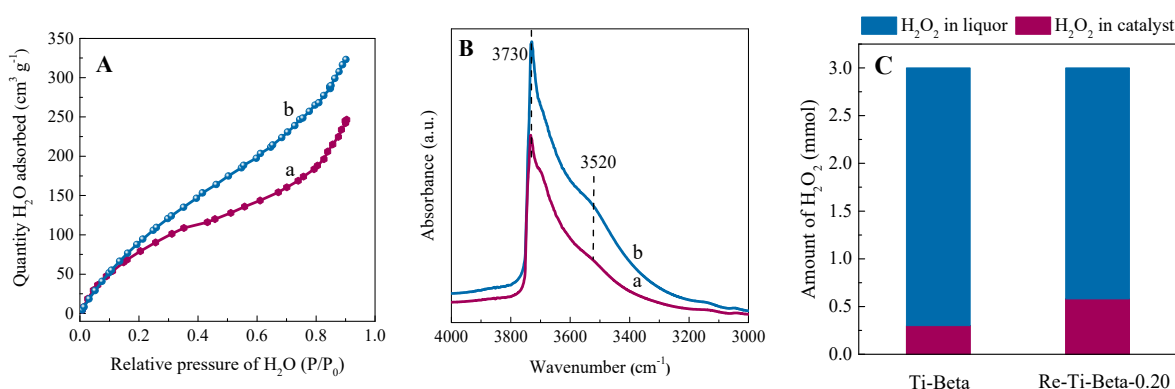
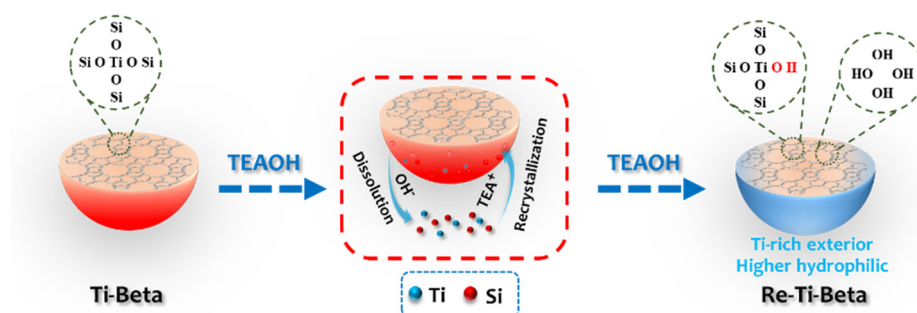


**Figure 9.**  $\text{H}_2\text{O}$  adsorption isotherms (A) and FT–IR spectra (B) in the hydroxyl stretching region of Ti–Beta (a) and Re–Ti–Beta–0.20 (b) at 298 K. The adsorption (C) of  $\text{H}_2\text{O}_2$  on Ti–Beta and Re–Ti–Beta–0.20. Adsorption conditions: 50 mg of dried catalyst; 3 mmol  $\text{H}_2\text{O}_2$  in MeCN, 5 mL; temp., 273 K (ice–water bath); time, 1 h.

Based on the careful characterization of the modification process and the obtained Re–Ti–Beta, it could be concluded that a good balance between the dissolution and recrystallization was achieved by tailoring the treatment condition, resulting in Re–Ti–Beta with high crystallinity (Scheme 1). A similar modification has also been performed on the TS–1 zeolite, with the tetrapropylammonium hydroxide (TPAOH) solution [44]. Although the SDA–assisted dissolution–recrystallization processes of Ti–Beta and TS–1 are both able to enhance the catalytic activity, some differences between the two cases cannot be ignored. The appropriate amount of TEOAH in the modification of Ti–Beta was larger than that of TPAOH in the case of TS–1 [44,45]. Intracrystal mesopores were observed for the modified TS–1 zeolite, while the mesopores formed in the modification process were mainly intercrystal ones in Ti–Beta [45,46]. Moreover, the enrichment of Ti species in the modification of TS–1 was not observed [44]. This is probably because the larger 12 MR pores in Beta zeolite favored the diffusion of the dissolved Ti and Si species out of the pores and the recrystallization on the outer surface.



**Scheme 1.** Schematic description of the modification of Ti–Beta by TEOAH solution.

### 2.3. Catalytic Performance in the Cyclohexene Epoxidation Reaction

As has been revealed in Figure 1B, the catalytic performance of Re–Ti–Beta–0.20 was superior to that of the pristine Ti–Beta in the cyclohexene epoxidation reaction. In a typical run, the CHE and H<sub>2</sub>O<sub>2</sub> conversion increased from 14.1% and 34.7% for Ti–Beta to 27.9% and 52.7% for Re–Ti–Beta–0.20. The H<sub>2</sub>O<sub>2</sub> utilization efficiency was also increased slightly from 40.6% to 52.9%. The kinetic profiles of cyclohexene epoxidation catalyzed by Ti–Beta and Re–Ti–Beta in the temperature range of 313–343 K were recorded. As shown in Figure 10A,B, the logarithm of the ratio of CHE concentration at “t” time to “0” time ( $-\ln\frac{[CHE]_t}{[CHE]_0}$ ) is plotted against the reaction time. A good linear relationship was observed, indicating that cyclohexene epoxidation is a first-order reaction [47]. The values of reaction rate constant ( $k$ ) at different reaction temperatures based on the slope of the curves in Figure 10A,B are listed in Table S1. The apparent activation energies ( $E_a$ ) of Ti–Beta and Re–Ti–Beta–0.20 in the temperature range of 313–343 K were further calculated by using the Arrhenius equation  $k = e^{\frac{-E_a}{RT}}$  (Figure 10C). The result showed that the  $E_a$  value of Ti–Beta (35.35 kJ mol<sup>-1</sup>) was higher than that of Re–Ti–Beta–0.20 (31.72 kJ mol<sup>-1</sup>), indicating that the modification process assisted by the TEAOH treatment reduced the apparent activation energy, resulting in enhanced activity in the cyclohexene epoxidation reaction. The above-detailed characterizations revealed that the Ti-rich exterior, the improved hydrophilicity and the formation of open Ti species all contributed to the enhanced activity of Re–Ti–Beta.

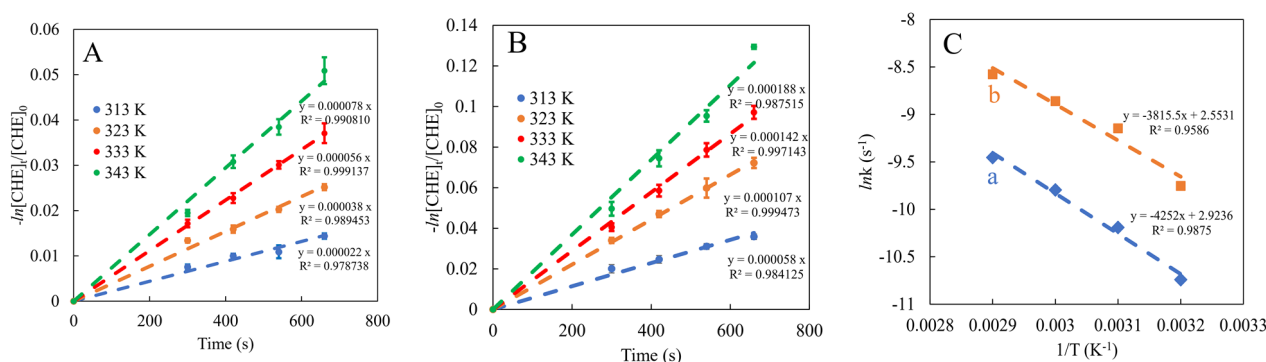


**Figure 10.** Kinetic analysis of cyclohexene epoxidation over Ti–Beta (A) and Re–Ti–Beta (B). Plots of apparent activation energy (C) in the cyclohexene epoxidation catalyzed by Ti–Beta (a) and Re–Ti–Beta–0.20 (b) catalysts. Reaction conditions: catalyst, 0.05 g; cyclohexene, 10 mmol; H<sub>2</sub>O<sub>2</sub> (30 wt.%), 10 mmol; MeCN, 10 mL.

To develop a highly active Ti–zeolite/H<sub>2</sub>O<sub>2</sub> catalytic system for the epoxidation of cyclohexene, the reaction conditions were further investigated for the Re–Ti–Beta–0.20 catalyst. As depicted in Figure 11A and Figure S4, the CHE and H<sub>2</sub>O<sub>2</sub> conversion and the effective utilization of H<sub>2</sub>O<sub>2</sub> were all increased with the increase in the catalyst amount from 0.05 to 0.20 g. However, the hydrolysis of CHO was also promoted along with the increase in catalyst amount due to the introduction of more Ti–related Lewis acid sites (Figure 11A), which favored the side reactions and reduced the CHO selectivity. The effect of reaction time on the cyclohexene epoxidation was subsequently investigated at 333 K over Re–Ti–Beta–0.20 catalyst. As shown in Figure 11B, with the prolonging of reaction time from 0.5 to 4 h, the CHE conversion increased from 14.8% to 33.1%. In addition, the H<sub>2</sub>O<sub>2</sub> conversion increased from 31.1% to 65.7% (Figure S5A), whereas the CHO selectivity slightly decreased from 87.5% to 76.4% (Figure 11B) with prolonging of the reaction time, indicating that the ring–opening reaction of CHO and deep oxidation of CHE might occur, generating by–products. The H<sub>2</sub>O<sub>2</sub> utilization efficiency exhibited a volcano–type change (Figure S5B). Moreover, the decline in H<sub>2</sub>O<sub>2</sub> utilization efficiency at longer reaction times was probably caused by pore blockage, which promoted the ineffective decomposition of H<sub>2</sub>O<sub>2</sub>. The reaction temperature also had a significant effect on the catalytic performance. It

was obvious that higher reaction temperature favored higher CHE conversion (Figure 11C) and H<sub>2</sub>O<sub>2</sub> conversion and utilization efficiency (Figure S6) but lower CHO selectivity (Figure 11C) for Re–Ti–Beta–0.20; thus, it could be deduced that high temperature easily promoted the hydrolysis of CHO.

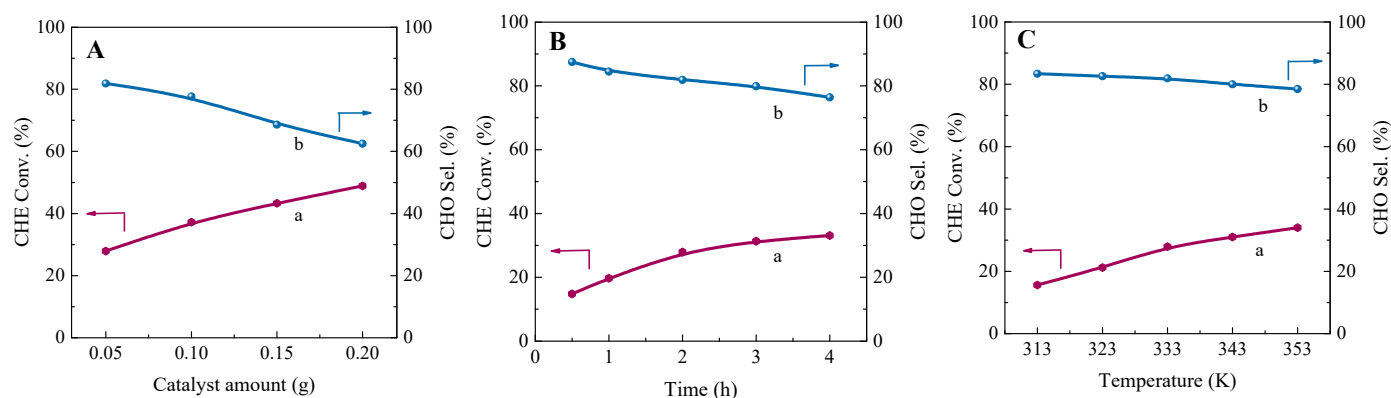


**Figure 11.** Dependence of CHE conversion (a) and CHO selectivity (b) on the catalyst amount (A), reaction time (B) and reaction temperatures (C) over Re–Ti–Beta–0.20. Reaction conditions: CHE, 10 mmol; H<sub>2</sub>O<sub>2</sub> (30 wt.%), 10 mmol; MeCN, 10 mL.

#### 2.4. The Reusability of Re–Ti–Beta

To evaluate the reusability of Re–Ti–Beta–0.20, the used catalysts were recovered by acetone washing and then reused for the epoxidation of cyclohexene again. As shown in Figure 12A, the CHE conversion decreased from 27.9% to 19.6% compared with fresh catalyst, and in the third run, the CHE conversion rate was 12.3%, while the CHO selectivity was maintained at 82%. After four runs, the catalyst was regenerated by calcination in air at 823 K for 6 h, and the reactivity was restored in the fifth run, with the activity comparable to that of the fresh catalyst. Compared with the fresh catalyst, the crystallinity of the spent Re–Ti–Beta–0.20 catalyst was decreased after four runs but could be completely recovered after calcination (Figure 12B). As shown in Figure 12C, the TG curve of the spent catalyst after four runs had two weight loss stages in the temperature range of 298–1000 K, and the weight loss in the high-temperature region (473–1073 K) was attributed to the decomposition of organics, accounting for 13.4 wt.%. After four runs, the Ti amount in fresh Re–Ti–Beta–0.20 (Si/Ti = 26.6) hardly changed, as indicated by the similar bulk Si/Ti molar ratio in the spent Re–Ti–Beta–0.20 (Si/Ti = 30.6). No significant difference in coordination states of Ti species between the fresh and regenerated catalysts was observed (Figure 12D), confirming that the Ti active center was robust in the epoxidation of cyclohexene reaction. It could be concluded from the above analysis that Re–Ti–Beta–0.20 is a reusable catalyst for cyclohexene epoxidation, and its deactivation was mainly caused by carbon deposition.

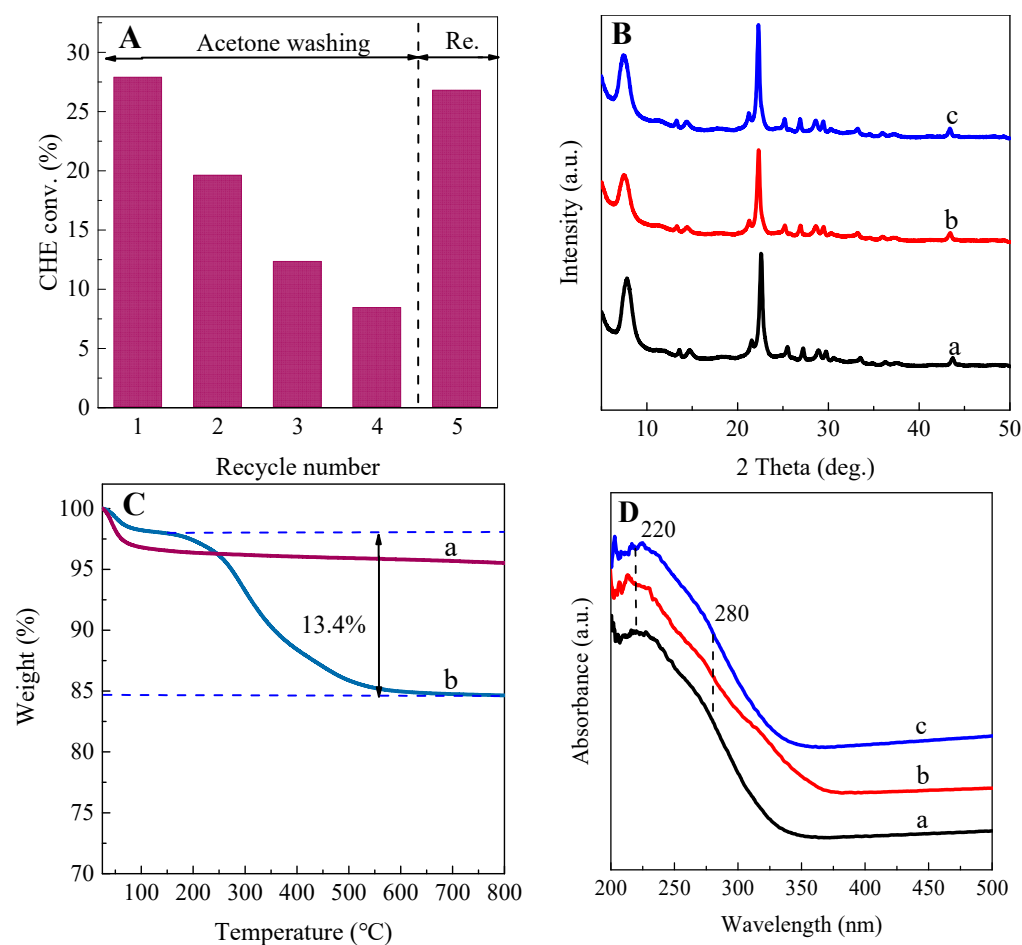


**Figure 12.** The recycling and regeneration (A) of Re–Ti–Beta–0.20 in cyclohexene epoxidation. XRD patterns (B), TG curves (C) and UV–Vis spectra (D) of fresh (a), spent (b) and regenerated (c) Re–Ti–Beta–0.20. The catalyst was washed with acetone three times after each reaction run and finally regenerated by calcination in air at 823 K for 6 h.

### 3. Materials and Methods

#### 3.1. Chemicals

The chemicals, including commercial Beta zeolite (Si/Al molar ratio = 11, Shanghai Xinnian Petrochemical Additives Co., Ltd, Shanghai, China.), nitric acid (HNO<sub>3</sub>, 65%, Sinopharm Chemical Reagent Co., Ltd, Shanghai, China.), tetraethylammonium hydroxide (TEAOH, 35%, SACHEM chemistry Co., Ltd, USA.), titanium butoxide (TBOT, 98%, Sinopharm Chemical Reagent Co., Ltd, Shanghai, China.), ammonium fluoride (NH<sub>4</sub>F, 96%, Sinopharm Chemical Reagent Co., Ltd, Shanghai, China.) and cyclohexene (CHE, >99.0%, Macklin, Shanghai, China.), were all used as purchased.

#### 3.2. Catalyst Preparation

##### 3.2.1. Preparation of the Parent Ti–Beta Zeolite via Structural Reconstruction Method

The parent Ti–Beta zeolite was prepared following the procedures in the literature [22]. Typically, the commercial Beta zeolite (Si/Al = 11) was dealuminated with 13 M HNO<sub>3</sub> solution at 413 K for 24 h. The resultant product was then filtered, washed, dried and finally calcined at 823 K for 6 h. The dealumination and calcination process was repeated twice, and the resultant sample was named DeAl–Beta (Si/Al > 2000). Ti–Beta was prepared via a structural reconstruction method with TEAOH as the organic structure–directing agent (OSDA), DeAl–Beta as the silica source and NH<sub>4</sub>F as the crystallization–supporting agent. The synthetic gel with a molar composition of 1.0 SiO<sub>2</sub>:0.33 TBOT:0.6 TEAOH:4 H<sub>2</sub>O:0.4 NH<sub>4</sub>F was hydrothermally crystallized at 423 K for 24 h with a rotation rate of 10 rpm.

After crystallization, the product was filtered, washed with deionized water, dried at 353 K overnight and calcined at 823 K for 6 h. The obtained sample was denoted as Ti–Beta.

### 3.2.2. Preparation of Re–Ti–Beta by Post–Modification of Ti–Beta

The post–modification of Ti–Beta zeolite was performed in the TEAOH aqueous solution with the composition of 1.0 SiO<sub>2</sub>:(0.04–0.28) TEAOH:(24–60) H<sub>2</sub>O, where the silica was from Ti–Beta. The mixture was then heated at the desired temperature for 24 h under static conditions. The product was separated from the mixture by filtration, washed with deionized water and dried at 353 K overnight, and the obtained sample was further calcined at 823 K for 6 h to obtain Re–Ti–Beta–x (x represents the molar ratio of TEAOH/Si).

### 3.3. Characterization Methods

The X–ray diffraction (XRD) patterns were collected on a Rigaku Ultima IV X–ray diffractometer using Cu K $\alpha$  radiation ( $\lambda = 0.1541$  nm) at 35 kV and 25 mA to confirm the structure and evaluate the crystallinity. To determine the morphology, scanning electron microscopy (SEM) images were taken on a Hitachi S–4800 microscope. The transmission electron microscopy (TEM) images were taken on a JEOL–JEM–2100 microscope. The textural properties were analyzed by nitrogen sorption at 77 K on a BELSORP–MAX instrument after degassing at 573 K under vacuum for 6 h. The Brunauer–Emmett–Teller (BET) analysis was carried out using the data in the relative pressure region of  $P/P_0 = 0.05–0.25$ , which provided the specific surface area. The contents of Si and Ti were quantified by inductively coupled plasma (ICP) on a Thermo IRIS Intrepid II XSP atomic emission spectrometer after dissolving the samples in an aqueous HF solution. X–ray photoelectron spectroscopy (XPS) was performed with Al K $\alpha$  ( $h\nu = 1486.6$  eV) radiation on AXIS SUPRA Imaging Photoelectron Spectrometer (Kratos Analytical Ltd, Japan.). Charging effects were corrected by using the C 1s peak due to adventitious carbon with a fixed binding energy of 284.6 eV. The solid–state <sup>29</sup>Si MAS NMR spectra were recorded on a VARIAN VNMRS–400 WB NMR spectrometer using a 7.5 mm T3HX probe and single–pulse method. The Fourier transform infrared spectra (FT–IR) were recorded on a Nicolet Nexus 670 FT–IR spectrometer in the absorbance mode at a spectral resolution of 4 cm<sup>–1</sup>. The sample was pressed into a self–supported wafer. Then, the wafer was set in a quartz cell which was connected to a vacuum system and sealed with CaF<sub>2</sub> windows. The UV–visible (UV–vis) diffuse reflectance spectra were obtained on a Shimadzu UV–2700 spectrophotometer using BaSO<sub>4</sub> as the reference in the region of 190–500 nm. The UV resonance Raman spectra (UVRRS) were collected on a triple spectrograph Raman system UV–Raman–100 with the excitation line at 244 nm and spectral resolution of 3 cm<sup>–1</sup>. The contents of water and organic species occluded in the samples were determined by the thermogravimetric (TG) analysis on a METTLER TOLEDO TGA/SDTA 851e instrument from 298 to 1073 K with a heating rate of 10 K min<sup>–1</sup> in air.

### 3.4. Liquid–Phase Epoxidation of Cyclohexene

The liquid–phase cyclohexene epoxidation reaction was carried out in a glass tube equipped with a condenser. In a typical run, 50 mg catalyst, 10 mmol cyclohexene, 10 mL acetonitrile (MeCN) and 10 mmol H<sub>2</sub>O<sub>2</sub> (30 wt.%) were mixed in the reaction tube and stirred vigorously at 333 K for 2 h. After the reaction, the reaction mixture was cooled with ice water, and then the catalyst was separated from the reaction system by centrifugation. The liquid–phase products were analyzed using a gas chromatograph (Shimadzu 2014, FID detector) equipped with an Rtx–Wax capillary column, and the generated products were identified by GC–MS (Agilent 6890 series GC system, 5937 network mass selective detector). The remaining amount of H<sub>2</sub>O<sub>2</sub> was determined by the titration method with 0.035 M Ce(SO<sub>4</sub>)<sub>2</sub> aqueous solution.

#### 4. Conclusions

Based on the above results and discussions, four points are summarized as follows:

(1) Highly hydrophilic Re–Ti–Beta zeolite with a Ti–rich exterior was synthesized by post–treating the parent Ti–Beta, which experienced a dissolution and recrystallization process in the TEAOH solution at elevated temperature. The optimized treatment conditions were carefully determined to produce Re–Ti–Beta zeolite with higher catalytic performance in the epoxidation reaction of cyclohexene.

(2) In a typical run of the cyclohexene epoxidation reaction, the CHE and H<sub>2</sub>O<sub>2</sub> conversion increased from 14.1% and 34.7% for Ti–Beta to 27.9% and 52.7% for Re–Ti–Beta–0.20.

(3) With a comprehensive analysis of the characterization results, three main factors are considered to contribute to the enhanced catalytic performance of Re–Ti–Beta, including the enhanced accessibility of Ti active sites due to the Ti–rich exterior, the enrichment of H<sub>2</sub>O<sub>2</sub> ascribed to higher hydrophilicity and the generation of more active open Ti species.

(4) The facial synthesis of parent Ti–Beta zeolite and the fast post–treatment process by TEAOH solution make the industrialization of highly active Re–Ti–Beta zeolite possible. Moreover, Re–Ti–Beta zeolite has shown great potential in the epoxidation reaction of bulky alkenes due to the open porosity compared to other microporous titanosilicates. Last but not the least, the excellent reusability of Re–Ti–Beta zeolite via the regeneration of calcination also makes it a potential industrial catalyst for the epoxidation reactions, especially those involving bulky substrates.

**Supplementary Materials:** The following are available online at <https://www.mdpi.com/article/10.3390/catal12040434/s1>, Figure S1. XRD patterns of Re–Ti–Beta–0.04 (A) and Re–Ti–Beta–0.20 (B) postsynthesized for a different crystallization time of 0 h (a), 1 h (b), 4 h (c), 8 h (d), 12 h (e), 16 h (f), 20 h (g), 24 h (h); Figure S2. The TEM images of pristine Ti–Beta (a) and Re–Ti–Beta–0.20 (b); Figure S3. TG curves of Ti–Beta (a) and Re–Ti–Beta–0.20 (b) after adsorption of water vapor provided by saturated NH<sub>4</sub>Cl solution at 293 K for 24 h; Figure S4. Dependence of H<sub>2</sub>O<sub>2</sub> conversion (A) and H<sub>2</sub>O<sub>2</sub> efficiency (B) on the amount of Re–Ti–Beta–0.20. Reaction conditions: CHE, 10 mmol; H<sub>2</sub>O<sub>2</sub> (30 wt.%), 10 mmol; MeCN, 10 mL; temp., 333 K; time, 2 h; Figure S5. Dependence of H<sub>2</sub>O<sub>2</sub> conversion (A) and H<sub>2</sub>O<sub>2</sub> efficiency (B) on the reaction time over Re–Ti–Beta–0.20. Reaction conditions: catalyst, 50 mg; CHE, 10 mmol; H<sub>2</sub>O<sub>2</sub> (30 wt.%), 10 mmol; MeCN, 10 mL; temp., 333 K; Figure S6. Dependence of H<sub>2</sub>O<sub>2</sub> conversion (A) and H<sub>2</sub>O<sub>2</sub> efficiency (B) at different reaction temperatures over Re–Ti–Beta–0.20. Reaction conditions: catalyst, 50 mg; CHE, 10 mmol; H<sub>2</sub>O<sub>2</sub> (30 wt.%), 10 mmol; MeCN, 10 mL; time, 2 h; Table S1. The average values of reaction rate constants (k) at different reaction temperatures of Ti–Beta and Re–Ti–Beta–0.20 in cyclohexene epoxidation.

**Author Contributions:** Formal analysis, H.P., R.P. and Z.Z.; funding acquisition, H.X. and P.W.; investigation, H.P.; project administration, M.H.; supervision, H.X. and P.W.; writing—original draft, H.P.; writing—review and editing, H.X. and P.W. All authors have read and agreed to the published version of the manuscript.

**Funding:** This research was funded by the National Key R & D Program of China (2021YFA1501401), National Natural Science Foundation of China (21872052 and 21972044) and Fundamental Research Funds for the Central Universities.

**Data Availability Statement:** All relevant data are included in the paper.

**Conflicts of Interest:** There are no conflicts of interest to declare.

#### References

1. Takeuchi, Y.; Asano, T.; Tsuzaki, K.; Wada, K. Catalytic asymmetric amination of meso–epoxide using soy polysaccharide (soyafibe S–DN). *Bull. Chem. Soc. Jpn.* **2018**, *91*, 678–683. [CrossRef]
2. Deng, T.; Zhao, G.F.; Liu, Y.; Lu, Y. Catalytic distillation for one–step cyclohexyl acetate production and cyclohexene–cyclohexane separation via esterification of cyclohexene with acetic acid over microfibrinous–structured Nafion–SiO<sub>2</sub>/SS–fiber packings. *Chem. Eng. Process.* **2018**, *131*, 215–226. [CrossRef]
3. Chan, H.Y.; Nguyen, V.H.; Wu, J.C.S.; Calvino–Casilda, V.; Bañares, M.A.; Bai, H. Real–Time Raman Monitoring during Photocatalytic Epoxidation of Cyclohexene over V–Ti/MCM–41 Catalysts. *Catalysts* **2015**, *5*, 518–533. [CrossRef]
4. Zhang, W.Z.; Guan, X.Z. Studies on the electrochemical epoxidation of cyclohexene. *Chem. J. Chinese, U.* **1998**, *10*, 1260–1262.

5. Rogers, O.; Pattison, S.; Macginley, J.; Engel, R.V.; Whiston, K.; Taylor, S.H.; Hutchings, G.J. The Low Temperature Solvent-Free Aerobic Oxidation of Cyclohexene to Cyclohexane Diol over Highly Active Au/Graphite and Au/Graphene Catalysts. *Catalysts* **2018**, *8*, 311. [[CrossRef](#)]
6. Zhou, X.T.; Ji, H.B.; Xu, J.C.; Pei, L.X.; Yao, X.D. Enzymatic-like mediated olefins epoxidation by molecular oxygen under mild conditions. *Tetrahedron Lett.* **2007**, *48*, 2691–2695. [[CrossRef](#)]
7. Aktas, A.; Saka, E.T.; Biyiklioglu, Z.; Acar, I.; Kantekin, H. Investigation of catalytic activity of new co (II) phthalocyanine complexes in cyclohexene oxidation using different type of oxidants. *J. Organomet. Chem.* **2013**, *745*, 18–24. [[CrossRef](#)]
8. Taramasso, M.; Perego, G.; Notari, B. Preparation of Porous Crystalline Synthetic Material Comprised of Silicon and Titanium Oxides. U.S. Patent 4410501, 13 October 1983.
9. Wu, P.; Tatsumi, T.; Komatsu, T.; Yashima, T. Hydrothermal synthesis of a novel titanosilicate with MWW topology. *Chem. Lett.* **2000**, *29*, 774–775. [[CrossRef](#)]
10. Wu, P.; Komatsu, T.; Yashima, T. Characterization of titanium species incorporated into dealuminated mordenites by means of IR spectroscopy and <sup>18</sup>O-exchange technique. *J. Phys. Chem.* **1996**, *100*, 10316–10322. [[CrossRef](#)]
11. Jappar, N.; Xia, Q.H.; Tatsumi, T. Oxidation activity of Ti-Beta synthesized by a dry-gel conversion method. *J. Catal.* **1998**, *180*, 132–141. [[CrossRef](#)]
12. Morey, M.S.; O'Brien, S.; Schwarz, S.; Stucky, G.D. Hydrothermal and postsynthesis surface modification of cubic, MCM-48, and ultralarge pore SBA-15 mesoporous silica with titanium. *Chem. Mater.* **2000**, *12*, 898–911. [[CrossRef](#)]
13. Corma, A.; Navarro, M.T.; Perez-Pariente, J. Synthesis of an ultralarge pore titanium silicate isomorphous to MCM-41 and its application as a catalyst for selective oxidation of hydrocarbons. *Chem. Commun.* **1994**, 147–148. [[CrossRef](#)]
14. Corma, A.; Cambor, M.A.; Esteve, P.; Martinez, A.; Perezpariente, J. Activity of Ti-Beta catalyst for the selective oxidation of alkenes and alkanes. *J. Catal.* **1994**, *145*, 151–158. [[CrossRef](#)]
15. Van Der Waal, J.C.; Rigutto, M.S.; Van Bekkum, H. Zeolite titanium beta as a selective catalyst in the epoxidation of bulky alkenes. *Appl. Catal. A* **1998**, *167*, 331–342. [[CrossRef](#)]
16. Cambor, M.A.; Costantini, M.; Corma, A.; Gilbert, L.; Esteve, P.; Martínez, A.; Valencia, S. Synthesis and catalytic activity of aluminium-free zeolite Ti-β oxidation catalysts. *Chem. Commun.* **1996**, 1339–1340. [[CrossRef](#)]
17. Blasco, T.; Cambor, M.A.; Corma, A.; Esteve, P.; Martínez, A.; Prieto, C.; Valencia, S. Unseeded synthesis of Al-free Ti-β zeolite in fluoride medium: A hydrophobic selective oxidation catalyst. *Chem. Commun.* **1996**, 2367–2368. [[CrossRef](#)]
18. Blasco, T.; Cambor, M.A.; Corma, A.; Esteve, P.; Guil, J.M.; Martínez, A.; Perdigón-Melón, J.A.; Valencia, S. Direct synthesis and characterization of hydrophobic aluminum-free Ti-Beta zeolite. *J. Phys. Chem. B* **1998**, *102*, 75–88. [[CrossRef](#)]
19. Leng, K.Y.; Li, X.L.; Ye, G.; Du, Y.C.; Sun, Y.Y.; Xu, W. Ti-containing hierarchical Beta with highly active sites for deep desulfurization of fuels under mild conditions. *Catal. Sci. Technol.* **2016**, *6*, 7615–7622. [[CrossRef](#)]
20. Tang, B.; Dai, W.L.; Sun, X.M.; Guan, N.J.; Li, L.D.; Hunger, M. A procedure for the preparation of Ti-Beta zeolites for catalytic epoxidation with hydrogen peroxide. *Green Chem.* **2014**, *16*, 2281–2291. [[CrossRef](#)]
21. Krijnen, S.; Sánchez, P.; Jakobs, B.T.F.; Van Hooff, J.H.C. A controlled post-synthesis route to well-defined and active titanium Beta epoxidation catalysts. *Microporous Mesoporous Mater.* **1999**, *31*, 163–173. [[CrossRef](#)]
22. Wang, B.W.; Xu, H.; Zhu, Z.G.; Guan, Y.J.; Wu, P. Ultrafast synthesis of nanosized Ti-Beta via structural reconstruction method as efficient oxidation catalyst. *Catal. Sci. Technol.* **2019**, *9*, 1857–1866. [[CrossRef](#)]
23. Tao, Y.S.; Kanoh, H.; Abrams, L.; Kaneko, K. Mesoporemodified zeolites: Preparation, characterization, and applications. *Chem. Rev.* **2006**, *106*, 896–910. [[CrossRef](#)]
24. Peng, P.; Gao, X.H.; Yan, Z.F.; Mintova, S. Diffusion and catalyst efficiency in hierarchical zeolite catalysts. *Natl. Sci. Rev.* **2020**, *7*, 1726–1742. [[CrossRef](#)]
25. Kerstens, D.; Smeyers, B.; Van Waeyenberg, J.; Zhang, Q.; Yu, J.; Sels, B.F. State of the art and perspectives of hierarchical zeolites: Practical overview of synthesis methods and use incatalysis. *Adv. Mater.* **2020**, *32*, 2004690. [[CrossRef](#)]
26. Chen, L.H.; Sun, M.H.; Wang, Z.; Yang, W.; Xie, Z.; Su, B.L. Hierarchically structured zeolites: From design to application. *Chem. Rev.* **2020**, *120*, 11194–11294. [[CrossRef](#)]
27. You, Q.; Wang, X.; Wu, Y.S.; Bi, C.Y.; Yang, X.; Sun, M.; Zhang, J.B.; Hao, Q.Q.; Chen, H.Y.; Ma, X.X. Hierarchical Ti-beta with a three-dimensional ordered mesoporosity for catalytic epoxidation of bulky cyclic olefins. *New J. Chem.* **2021**, *45*, 10303. [[CrossRef](#)]
28. Ren, W.C.; Hua, Z.L.; Ge, T.G.; Zhou, X.X.; Chen, L.S.; Zhu, Y.; Shi, J.L. Post-synthesis of hierarchically structured Ti-β zeolites and their epoxidation catalytic performance. *Chinese J. Catal.* **2015**, *36*, 906–912. [[CrossRef](#)]
29. Werner, A.; Bludovsky, P.; Selzer, C.; Koch, U.; Giebler, L.; Oswald, S.; Kaskel, S. Hierarchical Ti-beta obtained by simultaneous desilication and titanation as an efficient catalyst for cyclooctene epoxidation. *ChemCatChem* **2017**, *9*, 3860–3869. [[CrossRef](#)]
30. Ordonsky, V.V.; Murzin, V.Y.; Monakhova, Y.V.; Zubavichus, Y.V.; Knyazeva, E.E.; Nesterenko, N.S.; Ivanova, I.I. Nature, strength and accessibility of acid sites in micro/mesoporous catalysts obtained by recrystallization of zeolite BEA. *Microporous Mesoporous Mater.* **2007**, *105*, 101–110. [[CrossRef](#)]
31. Yang, G.J.; Qiu, Z.Y.; Han, J.; Chen, X.X.; Yu, J.H. Fluoride etching opens the access for bulky molecules to active sites in microporous Ti-Beta zeolite. *Mater. Chem. Front.* **2020**, *4*, 2982–2989. [[CrossRef](#)]

32. Bregante, D.T.; Johnson, A.M.; Patel, A.Y.; Ayla, E.Z.; Cordon, M.J.; Bukowski, B.C.; Greeley, J.; Gounder, R.; Flaherty, D.W. Cooperative effects between hydrophilic pores and solvents: Catalytic consequences of hydrogen bonding on alkene epoxidation in zeolites. *J. Am. Chem. Soc.* **2019**, *141*, 7302–7319. [[CrossRef](#)]
33. Wei, Y.; Li, G.; Su, R.M.; Lu, H.; Guo, H.C. Ti–sites environment–mediated hierarchical TS–1 catalyzing the solvent–free epoxidation: The remarkably promoting role of alcohol modification. *Appl. Catal. A* **2019**, *582*, 117108. [[CrossRef](#)]
34. Ratnasamy, P.; Srinivas, D.; Knozinger, H. Active sites and reactive intermediates in titanium silicate molecular sieves. *Adv. Catal.* **2004**, *48*, 1–169.
35. Xu, L.; Huang, D.D.; Li, C.G.; Ji, X.Y.; Jin, S.Q.; Feng, Z.C.; Xia, F.; Li, X.H.; Fan, F.T.; Li, C.; et al. Construction of unique six–coordinated titanium species with an organic ligand in titanosilicate and their unprecedented high efficiency for alkenes epoxidation. *Chem. Commun.* **2015**, *51*, 9010–9013. [[CrossRef](#)]
36. Mao, J.B.; Liu, M.; Li, P.; Liu, Y.; Guo, X.W. Modification of micrometer–sized TS–1 with tetrapropylammonium hydroxide and its catalytic properties in hydroxylation of phenol and ammoxidation of methyl ethyl ketone. *J. Fuel Chem. Technol.* **2008**, *36*, 484–488.
37. Tozzola, G.; Mantegazza, M.A.; Ranghino, G.; Petrini, G.; Bordiga, S.; Ricchiardi, G.; Lamberti, C.; Zulian, R.; Zecchina, A. On the Structure of the Active Site of Ti–Silicalite in Reactions with Hydrogen Peroxide: A Vibrational and Computational Study. *J. Catal.* **1998**, *179*, 64–71. [[CrossRef](#)]
38. Nogier, J.P.; Millot, Y.; Man, P.P.; Méthivier, C.; Che, M.; Dzwigaj, S. Nature, Environment and Quantification of titanium species in TiSiBEA zeolites investigated by XRD, NMR, DR UV–Vis and XPS. *Catal. Lett.* **2009**, *130*, 588–592. [[CrossRef](#)]
39. Yu, Y.K.; Wang, R.; Liu, W.; Chen, Z.; Liu, H.X.; Huang, X.; Tang, Z.M.; Liu, Y.M.; He, M.Y. Control of Ti active–site microenvironment in titanosilicate catalysts and its effect on oxidation pathways. *Appl. Catal. A* **2021**, *610*, 117953–117962. [[CrossRef](#)]
40. Su, J.; Xiong, G.; Zhou, J.C.; Liu, W.H.; Zhou, D.H.; Wang, G.R.; Wang, X.S.; Guo, H.C. Amorphous Ti species in titanium silicalite–1: Structural features, chemical properties, and inactivation with sulfosalt. *J. Catal.* **2012**, *288*, 1–7. [[CrossRef](#)]
41. Li, C.; Xiong, G.; Xin, Q.; Liu, J.K.; Ying, P.L.; Feng, Z.C.; Li, J.; Yang, W.B.; Wang, Y.Z.; Wang, G.R.; et al. UV resonance raman spectroscopic identification of titanium atoms in the framework of TS–1 zeolite. *Angew. Chem. Int. Ed.* **1999**, *38*, 2220–2222. [[CrossRef](#)]
42. Bregante, D.T.; Flaherty, D.W. Impact of Specific Interactions among Reactive Surface Intermediates and Confined Water on Epoxidation Catalysis and Adsorption in Lewis Acid Zeolites. *ACS Catal.* **2019**, *9*, 10951–10962. [[CrossRef](#)]
43. Fang, X.Q.; Wang, Q.; Zheng, A.M.; Liu, Y.M.; Lin, L.F.; Wu, H.H.; Deng, F.; He, M.Y.; Wu, P. Post–synthesis, characterization and catalytic properties of fluorine–planted MWW–type titanosilicate. *Phys. Chem. Chem. Phys.* **2013**, *15*, 4930–4938. [[CrossRef](#)]
44. Zuo, Y.; Song, W.C.; Dai, C.Y.; He, Y.P.; Wang, M.L.; Wang, X.S.; Guo, X.W. Modification of small–crystal titanium silicalite–1 with organic bases: Recrystallization and catalytic properties in the hydroxylation of phenol. *Appl. Catal. A* **2013**, *453*, 272–279. [[CrossRef](#)]
45. Chen, L.; Zhang, X.; Han, Q.; Xu, L.J.; Zhang, S.Y.; Yuan, Y.Y.; Xu, L. Post–synthesis of hierarchical TS–1 and its unique catalytic performance in the direct hydroxylation of toluene. *Appl. Catal. A* **2020**, *598*, 117588–117596. [[CrossRef](#)]
46. Wang, B.R.; Peng, X.X.; Zhang, W.F.; Lin, M.; Zhu, B.; Liao, W.L.; Guo, X.H.; Shu, X.T. Hierarchical TS–1 synthesized via the dissolution–recrystallization process: Influence of ammonium salts. *Catal. Commun.* **2017**, *101*, 26–30. [[CrossRef](#)]
47. Levenspiel, O. *Chemical Reaction Engineering*, 3rd ed.; Oxford University Press: Oxford, UK, 1999.